Surface plasmons with a gap in a semiinfinite HgTe-CdTe superlattice

1989 J. Phys.: Condens. Matter 1 7619

(http://iopscience.iop.org/0953-8984/1/41/013)

J. Phys.: Condens. Matter **1** (1989) 7619–7625. Printed in the UK

Surface plasmons with a gap in a semi-infinite HgTe–CdTe superlattice

Danhong Huang†, Yun Zhu‡ and Shixun Zhou†

† Department of Physics, Fudan University, Shanghai, People's Republic of China

‡ Centre of Theoretical Physics, China Centre of Advanced Science and Technology (World Laboratory), Beijing, and Department of Physics, Fudan University, Shanghai, People's Republic of China

Received 27 September 1988

Abstract. The density–density correlation function has been calculated to study the bulk and surface plasmons in a semi-infinite HgTe–CdTe superlattice. Several new surface plasmon modes with a gap between bulk and surface branches for both intra- and inter-sub-band excitations are found, which make the observation of surface plasmons in a superlattice possible. The gap is explained as the additional surface Coulomb interaction at adjacent interfaces in the quantum wells, due to the breaking of translational symmetry in the superlattice direction.

The density–density correlation functions for the bulk, semi-infinite and finite type I and type II superlattices have been calculated [1–3]. Bulk plasmons have been observed experimentally [4–6] in light scattering experiments. Surface plasmons still await detection, because it is difficult to satisfy the condition that the wavevector q in an experiment is greater than a critical wavevector q^*. Moreover, because of the limited resolution of the Raman spectrum, we have not so far detected the surface plasmon modes in superlattice even in the case of a null critical wavevector [7].

The HgTe–CdTe superlattice is a kind of attractive material which consists of both a semi-metal and a wide-gap semiconductor. The Γ_6–Γ_8 energy bands in the HgTe layer are reversed, as shown in figure 1 of the preceding paper, in contrast with those in CdTe layer, to give a zero gap. The computations of the band structure of HgTe–CdTe superlattice given by the PWM [8], the LCAO method [9, 10] and the EFA [11, 12] show that the electron-like, heavy-hole-like and light-hole-like states are confined very well in the HgTe and CdTe layers [10, 13, 14]. The Γ_8 energy bands in the HgTe and the CdTe layers possess effective masses with opposite signs on each side of the interface, respectively, which directly leads to the formation of a quasi-interface state with its energy lying in the range $0 < E_i < \Lambda$, where $\Lambda = V_p$ is the separation of Γ_8 energy bands in the HgTe and CdTe layers. Clearly, the electrons in the HgTe layers will be in the quasi-interface states localised near the interface with energy $E_i < \Lambda$. Moreover, light holes in the CdTe layers will also form anomalous quasi-interface states localised near the interface, owing to the negative effective mass of the light hole. All these results are consequences of matching the bulk states belonging to the conduction band in HgTe

0953-8984/89/417619 + 07 $02.50

with those belonging to the light-hole valence band in CdTe. This match is only favourable when the bulk states to be connected are made up of atomic orbitals of the same symmetry type and the effective masses on the two sides of the interface have opposite signs. As a collective excitation model, we can treat the interface states in HgTe and CdTe layers as two different kinds of quasi-particle with effective masses m_e and m_{lh} separately, just as in the model given in [9, 11].

It is proved that the thickness of the materials HgTe and CdTe will mainly determine the widths of band gap and sub-bands, respectively. We assume that the layers of HgTe and CdTe have the same thickness $d/2$ and that d is smaller than the critical thickness $d_c = (2m_{lh}/m_e^2\Lambda)^{1/2}$ so that the superlattice will behave like a semiconductor. It appears that the interface states play a more important role in the HgTe–CdTe superlattice than in type I and type II superlattices. Also, we consider the motion of quasi-particles in the layers to be completely free. If d is not too small, we can neglect tunnelling effects coming from the overlap of interface states localised at adjacent interfaces in the quantum well. It should be noted that, when the planar wavevector $\boldsymbol{k}_\parallel$ is not very small, the hybridisation between the interface states and the heavy-hole-like states will affect the fundamental gap of the material, which contributes a great deal to the transport and to optical absorption [11]. We have partly taken this effect into consideration by using wavefunctions with a finite width of localisation at interfaces. If we confine the study of collective excitation to the case in which the transitions of single particles, are limited to the neighbourhood of the Γ point of energy bands in $\boldsymbol{k}$-space, we can neglect hybridisation in the band structure [11]. However, this hybridisation can be taken into account by using a two band tight-binding model.

We shall now discuss the linear response of the HgTe–CdTe superlattice to an external potential in the absence of a magnetic field. In our approximation given in § 1, the single-particle wavefunction in this model superlattice can be written as

$$|\boldsymbol{k}, n, j\rangle = \exp(\mathrm{i}\boldsymbol{k}\cdot\boldsymbol{r})\,\xi_n(z - jd/2). \tag{1}$$

Here $\boldsymbol{k}$ is a two-dimensional wavevector describing the planar motion in the x–y plane; j and n are the layer index and the sub-band index, respectively. We shall restrict ourselves to considering only interface states. The layers are labelled by an integer j; even-numbered layers will be taken to be HgTe layers, in which electrons are confined, while odd-numbered layers are CdTe layers, in which light holes are confined. The non-interacting single-particle energy is given by

$$E_{nj}(\boldsymbol{k}) = E_{nj} + \hbar^2k^2/2m_j. \tag{2}$$

The system consists of a semi-infinite array of quantum wells, which are embedded in a medium, occupying the half-space $z > -d/4$, with a frequency-dependent dielectric function

$$\varepsilon_S(\omega) = \varepsilon_\infty(\omega^2 - \omega_L^2)/(\omega^2 - \omega_T^2) \tag{3}$$

where we have taken into account the electron–phonon coupling by replacing the background dielectric constant ε_S with $\varepsilon_S(\omega)$ in equation (3) [2]. ω_L and ω_T are the longitudinal and transverse optical phonon frequencies. The other half-space is filled by an insulator with a dielectric constant ε_0. In this work, we assume that only the lowest sub-band is filled at $T = 0$, and the exchange–correlation potential V^{xc} is taken to be zero for convenience.

If we follow [3] with the random-phase approximation (RPA), the commonly used diagonal approximation [15] and the electric quantum limit, a lengthy manipulation will lead to

$$\chi(\boldsymbol{q}, \omega; z, z') = \sum_n \sum_{l,l'} \chi_n(l, l')\Phi_n\left(z - \frac{ld}{2}\right)\Phi_n\left(z' - \frac{l'd}{2}\right) \tag{4}$$

with

$$\Phi_n(z - jd/2) = \Psi_n(j, j; z) + [\Psi_n(j+1, j; z) + \Psi_n(j-1, j; z) + \Psi_n(j, j+1; z) + \Psi_n(j, j-1; z)]/2 \tag{5}$$

$$\Psi_n(j, j'; z) = \xi_n(z - jd/2)\,\xi_n(z - j'd/2) \tag{6}$$

$$\chi_n(l, l') = \chi_n^0(l, l)\delta_{ll'} + \sum_m \chi_n^0(l, l)V_{n,n}(l, m)\chi_n(m, l') \tag{7}$$

where $\chi_n^0 = \Pi_{0,n}^0 + \Pi_{n,0}^0$ for $n \neq 0$ and $\chi_0^0 = \Pi_{0,0}^0$ are the polarisabilities of the non-interacting system and $V_{n,n}(l, m)$ is the Coulomb interaction, including the effect of image charges and sub-band structure.

The Fourier tranform of equation (4) gives

$$\boldsymbol{\chi}_n(k, k') = \boldsymbol{\chi}_0\delta_{kk'} + V_q \sum_{k''} \boldsymbol{\chi}_0\,\mathbf{f}_{nn}(k, k'')\boldsymbol{\chi}_n(k'', k') \tag{8}$$

where $v_q = 2\pi e^2/\varepsilon_S(\omega)q$,

$$\boldsymbol{\chi}_0 = \begin{bmatrix} \chi_n^e & 0 \\ 0 & \chi_n^h \end{bmatrix} \tag{9}$$

$$\boldsymbol{\chi}_n(k, k') = \begin{bmatrix} \chi_n^{e\text{–}e}(k, k') & \chi_n^{e\text{–}h}(k, k') \\ \chi_n^{h\text{–}e}(k, k') & \chi_n^{h\text{–}h}(k, k') \end{bmatrix} \tag{10}$$

and $\mathbf{f}_{nn}(k, k')$ is the Fourier transform of the Coulomb interaction $\mathbf{V}_{nn}(l, l')$. Even and odd j refer to electron-like and light-hole-like states, respectively. We write $\boldsymbol{\chi}_n(k, k')$ and $\mathbf{f}_{nn}(k, k')$ in terms of the 'bulk' and 'surface' parts:

$$\boldsymbol{\chi}_n(k, k') = \boldsymbol{\chi}_n^B(k)\delta_{kk'} + \boldsymbol{\chi}_n^s(k, k') \tag{11}$$

$$\mathbf{f}_{nn}(k, k') = \mathbf{f}_n^B(k)\delta_{kk'} + \mathbf{f}_n^s(k, k') \tag{12}$$

where

$$\boldsymbol{\chi}_n^B(k) = [\mathbf{I} - \chi_0 v_q \mathbf{f}_n^B(k)]^{-1}\boldsymbol{\chi}_0 \tag{13}$$

$$\mathbf{f}_n^B(k) = \{\mathbf{r}_{-n}(q)[\exp(-ikd) - \exp(-qd)] + \mathbf{r}_{-n}(-q)[\exp(ikd) - \exp(-qd)]\}/2P(\boldsymbol{q}, k) + \mathbf{V}_{-n}(q) \tag{14}$$

with

$$\mathbf{r}_{\pm n}(q) = \begin{bmatrix} G_{\pm n}(q) & \exp(\mp qd/2)\, G_{\pm n}(q) \\ \exp(-qd/2)\, G_{\pm n}(q) & G_{\pm n}(q) \end{bmatrix} \tag{15}$$

$$\mathbf{V}_{-n}(q) = \begin{bmatrix} V_{-n}(q) & \exp(-qd/2)\, G_{-n}(q) \\ \exp(-qd/2)\, G_{-n}(q) & V_{-n}(q) \end{bmatrix} \tag{16}$$

where the symbols $G_{\pm n}(q)$ and $V_{-n}(q)$ are given by

$$G_{\pm n}(q) = \tfrac{1}{2}\int_{-d/4}^{\infty} \mathrm{d}z \int_{-d/4}^{\infty} \mathrm{d}z'\, \Phi_n(z)\Phi_n(z') \exp[-q(z \pm z')] \tag{17}$$

$$V_{-n}(q) = \tfrac{1}{2}\int_{-d/4}^{\infty} \mathrm{d}z \int_{-d/4}^{\infty} \mathrm{d}z'\, \Phi_n(z)\Phi_n(z') \exp[-q|z - z'|] \tag{18}$$

and $P(q, k) = \cosh(qd) - \cos(kd)$. Furthermore, we straightforwardly write down the surface part of Coulomb interaction:

$$\begin{aligned} \mathbf{f}_n\, s(k, k') = {} & \{[1 - \exp(-qdN)]/4NP(q, k)P(q, k')\} \\ & \times \{\mathbf{a} - \mathbf{b}_1 \exp(\mathrm{i}kd) - \mathbf{b}_2 \exp(-\mathrm{i}k'd) + \mathbf{c} \exp[\mathrm{i}(k - k')d]\} \end{aligned} \tag{19}$$

where

$$\mathbf{a} = [\mathbf{r}_{-n}(q) + \mathbf{r}_{-n}(-q)] + \alpha \mathbf{r}_{+n}(q) \exp(2qd) \tag{20}$$

$$\mathbf{b}_1 = [\mathbf{r}_{-n}(q) \exp(-qd) + \mathbf{r}_{-n}(-q) \exp(qd)] + \alpha \mathbf{r}_{+n}(q) \exp(qd) \tag{21}$$

$$\mathbf{b}_2 = [\mathbf{r}_{-n}(q) \exp(qd) + \mathbf{r}_{-n}(-q) \exp(-qd)] + \alpha \mathbf{r}_{+n}(q) \exp(qd) \tag{22}$$

$$\mathbf{c} = [\mathbf{r}_{-n}(q) + \mathbf{r}_{-n}(-q)] + \alpha \mathbf{r}_{+n}(q) \tag{23}$$

$$\alpha = [1 - \exp(-qdN)] \exp(-qd/2)[\varepsilon_S(\omega) - \varepsilon_0]/[\varepsilon_S(\omega) + \varepsilon_0]. \tag{24}$$

By using the *ansatz* for $\boldsymbol{\chi}_n^S(k, k')$ [3] in equations (8), (11) and (12), we obtain

$$\begin{aligned} \boldsymbol{\chi}_n^S(k, k') = {} & \{[1 - \exp(-qdN)]/4NP(q, k)P(q, k')\}\boldsymbol{\chi}_n^B(k) \\ & \times \{\mathbf{A} - \mathbf{B}_1 \exp(\mathrm{i}kd) - \mathbf{B}_2 \exp(-\mathrm{i}k'd) + \mathbf{C} \exp[\mathrm{i}(k - k')d]\}\boldsymbol{\chi}_n^B(k') \end{aligned} \tag{25}$$

with the coefficients given by the following equations:

$$\begin{bmatrix} \mathbf{A} \\ \mathbf{B}_1 \end{bmatrix} = \mathbf{M}^{-1} \begin{bmatrix} \mathbf{a} \\ \mathbf{b}_1 \end{bmatrix} \qquad \begin{bmatrix} \mathbf{B}_2 \\ \mathbf{C} \end{bmatrix} = \mathbf{M}^{-1} \begin{bmatrix} \mathbf{b}_2 \\ \mathbf{c} \end{bmatrix} \tag{26}$$

where

$$\mathbf{M} = \begin{bmatrix} \mathbf{I} - \mathbf{aG} - \mathbf{b}_2\mathbf{H}_- & \mathbf{aH}_+ - \mathbf{b}_2\mathbf{G} \\ \mathbf{cH}_- - \mathbf{b}_1\mathbf{G} & \mathbf{I} - \mathbf{cG} + \mathbf{b}_1\mathbf{H}_- \end{bmatrix} \tag{27}$$

$$\mathbf{G} = \frac{v_q[1 - \exp(-qdN)]}{4N} \sum_k \frac{\boldsymbol{\chi}_n^B(k)}{P(q, k)^2} \tag{28}$$

$$\mathbf{H}_\pm = \frac{v_q[1 - \exp(-qdN)]}{4N} \sum_k \frac{\exp(\pm \mathrm{i}kd)\boldsymbol{\chi}_n^B(k)}{P(q, k)^2}. \tag{29}$$

For a semi-infinite superlattice ($N \to \infty$), bulk plasmons are given by the poles of the bulk part (13), while surface plasmons are given by the poles of the surface part (25).

For intra-sub-band excitation, we have

$$\xi_0(z) = \begin{cases} D\exp(\beta d/4)[\exp(\beta z) + \exp(-\beta d)\exp(-\beta z)] & -3d/4 \leqslant z \leqslant -d/4 \\ D\exp(-\beta d/4)[\exp(\beta z) + \exp(-\beta z)] & -d/4 \leqslant z \leqslant d/4 \\ D\exp(\beta d/4)[\exp(-\beta z) + \exp(-\beta d)\exp(\beta z)] & d/4 \leqslant z \leqslant 3d/4 \end{cases} \tag{30}$$

with the normalisation factor

$$D = \exp(\beta d/4)/[d + 2\sinh(\beta d/2)/\beta]^{1/2} \tag{31}$$

and the long-wavelength form of $\chi_0^{e(h)}(\boldsymbol{q}, \omega)$ given by

$$\chi_0^{e(h)}(\boldsymbol{q}, \omega) = n_{e(h)}q^2/m_{e(h)}\omega^2. \tag{32}$$

The ratio of the plasma frequencies for the electron and hole layers is $\gamma = \omega_{pe}(q)^2/\omega_{ph}(q)^2$. On the contrary, for inter-sub-band excitation, we have

$$\xi_1(z) = \begin{cases} C\exp(-\beta d/4)\{\exp[-\beta(z + d/2)] - \exp[\beta(z + d/2)]\} & -3d/4 \leqslant z \leqslant -d/4 \\ C\exp(-\beta d/4)[\exp(\beta z) - \exp(-\beta z)] & -d/4 \leqslant z \leqslant d/4 \\ C\exp(-\beta d/4)\{\exp[-\beta(z - d/2)] - \exp[\beta(z - d/2)]\} & d/4 \leqslant z \leqslant 3d/4 \end{cases} \tag{33}$$

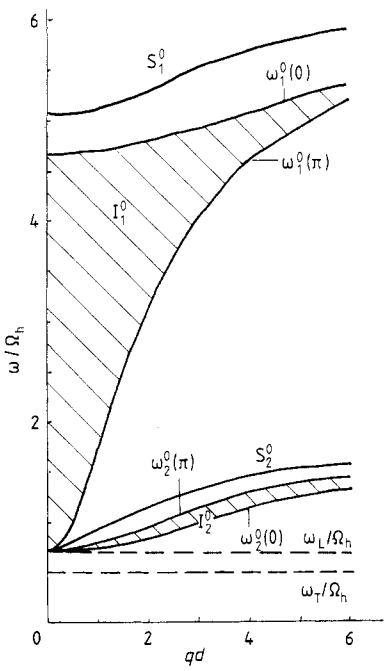

Figure 1. Two higher branches of the collective intra-sub-band excitation spectrum for phonon–plasmon modes in quasi-2D interfaces with the parameters $\beta d = 0.7742$, $\varepsilon_\infty = 16.0$, $\varepsilon_0 = 1.0$, $\gamma = 15.0$, $(\omega_L/\Omega_h)^2 = 0.5$, $(\omega_T/\Omega_h)^2 = 0.25$ and $\delta = d/4$.

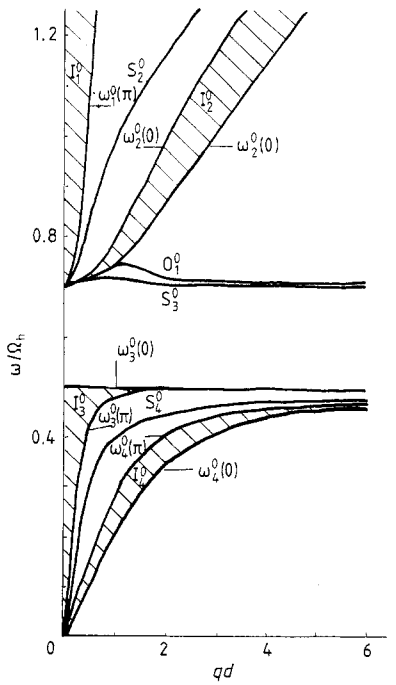

Figure 2. Two lower branches of the collective intra-sub-band excitation spectrum for phonon–plasmon modes in quasi-2D interfaces. The parameters are the same as in figure 1.

with the normalisation factor

$$C = \exp(\beta d/4)/[2\sinh(\beta d/2)/\beta - d]^{1/2} \tag{34}$$

and the long-wavelength form of $\chi_1^{e(h)}(q, \omega)$ to the order of q given by

$$\chi_1^{e(h)}(q, \omega) = 2n_{e(h)}\Omega_{10}/\hbar(\omega^2 - \Omega_{10}^2). \tag{35}$$

The ratio of the α-parameters is $\gamma' = \alpha_e/\alpha_h$.

All the results are presented in figures 1–4 for both intra- and inter-sub-band excitations.

From figures 1 and 2, we can see that there exist four bulk modes I_1^0–I_4^0 [16], two of which come from the splitting, owing to the electron–phonon coupling. The interaction between optical phonons and bulk plasmons is responsible for the optical phonon bands I_2^0 and I_3^0. I_1^0 and I_4^0 are optical and acoustical bulk plasmons, respectively. Moreover, there are two optical phonon–surface plasmon modes S_2^0 and S_3^0, one optical surface plasmon mode S_1^0 and one acoustical surface plasmon mode S_4^0. O_1^0 mode is a new optical phonon–surface plasmon mode in the intra-sub-band excitations, which, to our knowledge, has never been reported before. It should be noted that the existence of a gap between S_1^0 and I_1^0 modes can be explained as due to the additional surface Coulomb interaction between neighbouring interfaces.

From figures 3 and 4, we know that there are four bulk modes I_1^1–I_4^1 [17]. Of them,

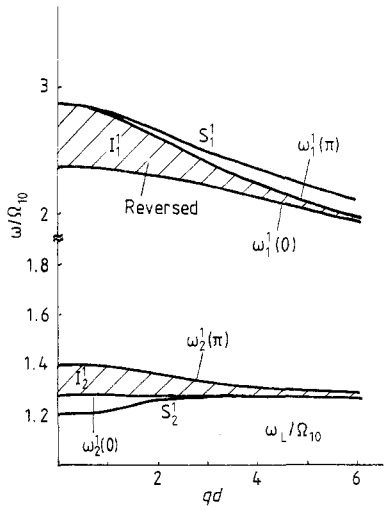

Figure 3. Two higher branches of the collective inter-sub-band excitation spectrum for phonon–plasmon modes in quasi-2D interfaces with the parameters $\beta d = 0.7742$, $\varepsilon_\infty = 16.0$, $\varepsilon_0 = 1.0$, $\gamma = 17.5$, $(\omega_L/\Omega_{10})^2 = 1.5$, $(\omega_T/\Omega_{10})^2 = 0.75$, $\alpha_h = 1.84$ and $\delta = d/4$.

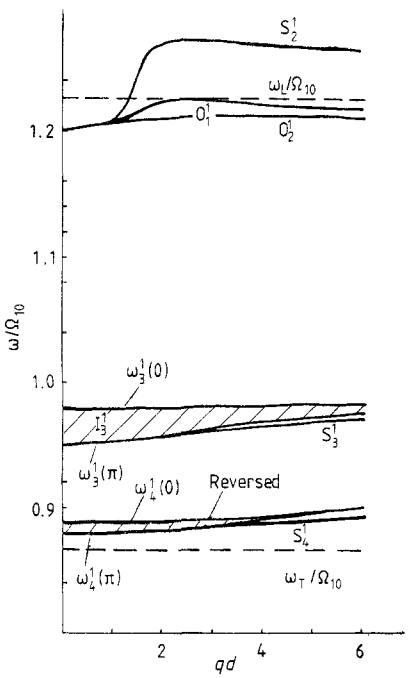

Figure 4. Two lower branches of the collective inter-sub-band excitation spectrum for phonon–plasmon modes in quasi-2D interfaces. The parameters are the same as in figure 3.

I_3^1 and I_4^1 are two optical phonon bands coming from the electron–phonon coupling. Also, there are two optical phonon–surface plasmon modes S_3^1 and S_4^1 as well as the other two surface modes S_1^1 and S_2^1 associated with inter-sub-band excitations. Note, however, that there are two extra modes O_1^1 and O_2^1 with frequencies below ω_L associated with the 0–1 inter-sub-band transition, in which the O_1^1 mode has been predicted in [2], while the O_2^1 mode is new and has not been reported previously. The dramatic feature is that a gap also exists between the S_2^1 and I_2^1 modes. The reason for the existence of this gap is analogous to that in the intra-sub-band excitation. We can easily see that both the I_1^1 and the I_4^1 modes are reversed in figures 3 and 4.

Acknowledgments

This work was supported in part by the Chinese Higher Education Foundation through Grant 2-1987 and in part by the Chinese Science Foundation through Grant 1860723.

References

[1] Jain J K and Allen P B 1985 *Phys. Rev.* B **32** 997
[2] Hawryiak P, Wu Ji-Wei and Quinn J J 1985 *Phys. Rev.* B **32** 5169
[3] Hawrylak P, Eliasson G and Quinn J J 1986 *Phys. Rev.* B **34** 5368
[4] Olego D, Pinczuk A, Gossard A C and Wiegmann W 1982 *Phys. Rev.* B **25** 7867
[5] Sooryakumar R, Pinczuk A, Gossard A C and Wiegmann W 1985 *Phys. Rev.* B **31** 2578
[6] Pinczuk A, Lamont M G and Gossard A C 1986 *Phys. Rev. Lett.* **56** 2092
[7] Zhu Yun, Cai Shengshen and Zhou Shixun 1989 *Phys. Rev.* B at press
[8] Mukherji D and Nag B R 1957 *Phys. Rev.* B **12** 4338
[9] Chang Y-C, Schulman J N, Bastard G, Guldner Y and Voos M 1985 *Phys. Rev.* B **31** 2557
[10] Jaros M, Zoryk A and Ninno D 1987 *Phys. Rev.* B **35** 8277
[11] Lin-Liu Y R and Sham L J 1985 *Phys. Rev.* B **32** 5561
[12] Bastard G 1982 *Phys. Rev.* B **25** 7584
[13] Kawamoto G H, Quinn J J and Bloss W L 1981 *Phys. Rev.* B **23** 1785
Dahl D L and Sham L J 1977 *Phys. Rev.* B **16** 651
[14] Berroir J M, Guldner Y and Voos M 1986 *IEEE J. Quantum Electron.* **QE-22** 1793
[15] Faurie J-P 1986 *IEEE J. Quantum Electron.* **QE-22** 1656
[16] Huang Danhong and Zhou Shixun 1988 *Phys. Rev.* B **38** 13061
[17] Huang Danhong and Zhou Shixun 1988 *Phys. Rev.* B **38** 13069